Open-source low-cost cardiac optical mapping system

Rybashlykov D.[1], Brennan J.[2], Lin Z[2]., Efimov I.R.[2,*], Syunyaev R.[1,#]

[1]Human Physiology Lab, Moscow Institute of Physics and Technology, Moscow, Russia
[2]Department of Biomedical Engineering, The George Washington University, Washington DC, USA

* Corresponding author 1

E-mail: irefimov@gmail.com

Corresponding author 2

E-mail: roman.syunyaev@gmail.com

Abstract

Fluorescent imaging with voltage- or calcium-sensitive dyes, *i.e.* optical mapping, is one of the indispensable modern techniques to study cardiac electrophysiology, unsurpassed by temporal and spatial resolution. High-speed CMOS cameras capable of optical registration of action potential propagation are in general very costly. We present a complete solution priced below US$1,000 (including camera and lens) at the moment of publication with an open-source image acquisition and processing software. We demonstrate that the iDS UI-3130CP rev.2 camera we used in this study is capable of 200x200 977 frames per second (FPS) action potential recordings from rodent hearts. The signal-to-noise-ratio of a conditioned signal was 16 ± 10 for rodent hearts. A comparison with a specialized MiCAM Ultimate-L camera has shown that signal-to-noise ratio (SNR) is sufficient for accurate measurements of AP waveform, conduction velocity (± 0.04 m/s) and action potential duration (± 7ms) in mouse and rat hearts. We measured the action potential prolongation during 4-aminopyridine administration in mouse heart, showing that proposed system signal quality is adequate for drug studies.

Introduction

An optical technique of measurement of cellular transmembrane voltage *via* potentiometric dyes was introduced in the 1970s, known today as optical mapping [1-4]. Potentiometric dye molecules bind to cell membranes and undergo either molecular motion or an electronic redistribution upon excitation and emission [5]. The changes of the external electrical field affect transition energy, corresponding emission spectrum can be detected and recorded. Further advances in the field include calcium-sensitive dyes (changing emission spectrum upon binding with calcium ions) [6], metabolic imaging (*via* intrinsic NADH fluorescence) [7], simultaneous mapping of voltage and calcium [8,9], simultaneous imaging from the several sides of the heart (panoramic mapping) [10,11], and transmural imaging via long wavelength dyes [12].

One particular advantage of optical mapping in comparison to traditional multielectrode arrays is high spatial and temporal resolution that makes it possible to accurately track the

rapidly propagating excitation wavefronts in ventricular and atrial arrhythmias [13]. However high spatio-temporal resolution requires highly specialized cameras: 100x100 pixels, 1,000 frames per second (FPS) and digital image acquisition hardware. It typically has a high price of US$50,000-100,000. This price is prohibitively high for education and some research applications, for example, several cameras are required for multiparametric and panoramic optical mapping. Recently, high speed USB 3.0 computer vision-specialized industrial CMOS cameras entered the mass market eliminating the need for specialized data-acquisition systems and, thus, reducing the price of a fast imaging system. Previously, Lee et al. [14] have demonstrated that it is possible to optically map pig and rabbit hearts with relatively inexpensive ($600-1200) CMOS cameras, as it was possible with inexpensive CCD cameras [15]. In particular, Lee et al. have shown that action potential (AP) recordings up to 1,000 Hz and SNR of up to ~50 (defined as (AP Amplitude)/(SD during diastolic intervals)) are possible in large animal hearts with USB3.0 iDS (Imaging Development Systems, GmbH) cameras. Unfortunately, this method was not applied to rodents, which are much more popular models compared to pigs and rabbits, and not made available to the wider research community.

In our open-source research and development presented here we used iDS UI-3130CP-M-GL (~$700US including lens) and iDS Software Suite programming interface that makes it possible to customize image acquisition (Fig 1). Here, we demonstrate capabilities of action potential recordings in the two most widespread laboratory animal models: rat and mouse hearts. Small rodent hearts are more challenging for optical recordings as compared to large animal hearts due to much lower optical signal intensity. We compared this inexpensive solution to the state-of-the-art MiCAM ULTIMA-L system, which has superior SNR (Fig 2), but at a much higher price of approximately $100,000. New inexpensive optical mapping system provides sufficient quality data to track activation and repolarization sequences and action potential duration (APD).

Fig 1. The experimental setup for the iDS camera. (A) iDS UI-3130CP M.GL camera (977Hz sampling frequency). (B) Pentax C60607KP. (C) 650nm long-pass filter. (D) Green excitation LED (530nm wavelength). (E) Perfusion chamber with heart. (F) **iDS** Recorder application. (G) Open source RHYTHM1.2 software, based on Matlab and C++.

Fig 2. Histogram of SNR in recordings from mouse ventricles (n=6). Orange

represents SNR of the raw signal obtained by iDS, green represents SNR from the same pixels after signal conditioning, blue represents corresponding SNR of the raw signal obtained by MiCAM.

Materials and Methods

iDS UI-3130CP camera and software

In this study a UI-3130CP camera from Imaging Development Systems was used. It is capable of 10 bit recordings at resolutions up to 800 by 600 pixels. The "uEye cockpit" image acquisition software provided by iDS has neither an option to save recordings in lossless format, nor an option to make 10 bit recordings. Therefore we have developed a custom open-source image acquisition application using the C++ API provided by iDS (*https://github.com/humanphysiologylab/ueyemappingWin*).

The custom software was designed to make recordings with a resolution of 200x200 pixels and a framerate of 977 frames per second (FPS). The high frequency recordings were possible because of the reduction of the active part of the sensor to the smaller area in the center. Although the framerate up to 1400 FPS is possible at 120x120 pixels resolution, this resulted in a narrow (5.5 degrees) field of view. Since direct capture to solid-state drive resulted in frame loss and uneven FPS, software was designed to capture the recording directly to the RAM and to transfer it to the storage after the recording has finished. This approach requires RAM size large enough to store the whole recording. For example, a 5 second recording at 200x200 resolution at 977 FPS requires 375 MB of memory. Considering this data memory requirement, at least 2 GB of RAM is recommended. The software interface allows users to visualize signal intensity and change the recording gain and frame rate before the image acquisition (S1 Fig), which is essential to adjust LED intensity when signal intensity is too low or saturated. The file format of the data is covered in the software user manual. Binary iDS camera recordings are compatible with popular open-source RHYTHM signal processing and analysis software [9], which we update regularly.

Optical mapping protocol

All experimental protocols were approved by the Institutional Animal Care and Use Committee at The George Washington University and conform to the NIH Guide for the Care and Usage of Laboratory animals.

We followed the protocol described earlier [16]. Briefly, animals were anesthetized via isoflurane vapors, after ensuring thoracotomy heart was excised and cannulated. Hearts were Langendorff-perfused with Tyrode's solution (in mM: 128.2 NaCl, 4.7 KCl, 1.05 MgCl2, 1.3 CaCl2, 1.19 NaH2PO4, 20 NaHCO3, 11.1 Glucose), electromechanically uncoupled with 5-10 μM blebbistatin and stained with voltage-sensitive dye Di-4-ANEPPS. Left ventricle was paced at 80 - 150 ms pacing cycle length (PCL), PCL of 150 ms was fast enough to suppress sinus rhythm in all experiments. The dye was excited with 520 nm LED (Prizmatix UHP-Mic-LED-520), and fluorescent emission was captured through a long-pass filter (650nm) (Fig 1). Resulting optical signal was recorded sequentially by either the iDS camera or the MiCAM from the same camera position: after recording several sequences at varying pacing cycle lengths (PCL), it was removed, and the iDS camera was installed in its place (Fig 1).

Pharmacological protocol

4-Aminopyridine (4-AP), a transient outward current (I_{to}) blocker [17–24], was purchased from Millipore Sigma (Cat. 278575). 250 mM 4-AP stock solution. It was prepared with pH adjusted to 7.4 using 1 M hydrochloric acid (Fisher Scientific, SA48-1). Small quantities of the 4-AP stock solution were added to the modified Tyrode's perfusion solution and perfused for 10 min to reach a final working concentration of 5.6 mM.

Data conditioning and analysis

Signal conditioning included ensemble averaging both in space (gaussian filter with window of 3 by 3 pixels for MiCAM and 5 by 5 pixels for iDS) and in time (all beats were averaged in a 2 s recording). Conduction velocity was calculated using RHYTHM 1.2 [9]. with the algorithm earlier described by Bayly et al [25]. Signal-to-noise ratio (SNR) was calculated as the ratio of the root mean square amplitude to the root mean square noise, where the

amplitude of noise is evaluated at resting potential.

APD was measured at 80 % repolarization (APD80). The noise amplitude affected apparent resting potential in the recordings, hampering the comparison of APD80 measured by two cameras. Therefore, prior to APD calculation, resting potential level for each pixel was determined by gaussian filter ($\boldsymbol{\sigma}$ = 7ms, truncated at $\boldsymbol{4*\sigma}$). Prior to APD calculations, noisy and oversaturated areas were excluded semi-automatically by choosing appropriate SNR and signal intensity cutoff levels.

Signal processing and analysis were done with Rhythm 1.2 software [9], while APD and SNR comparison between two cameras were done as described above with custom python scripts.

Results

The capabilities and limitations of the iDS camera system were tested in comparison with the more expensive state-of-the-art MiCAM Ultimate-L system on Langendorff-perfused mouse and rat hearts. We used the traditional optical mapping setup [16] shown on Fig 1 (see "Materials and Methods" for details on signal acquisition and processing). Raw iDS signal recordings were, in general, quite noisy: SNR was 0.5 ± 0.4 for mouse hearts (Fig 2, S2 Fig; here and below standard errors are reported). Signal processing (binning and ensemble averaging, see Methods for details) increased SNR to 16 ± 10 for the mouse heart. The comparison of representative iDS and MiCAM optical mapping systems recordings are shown in Fig 3C-H, Fig 4C-H. The processed signal clearly reproduces both depolarization phase and general AP waveform.

Fig 3. Conditioned signals in recordings of a mouse heart. (A),(B) Still frames with color-coded pixels corresponding to the AP waveforms. (C),(E),(G) Signals obtained from iDS camera. (D),(F),(H) Signals obtained from the MiCAM camera.

Fig 4. Conditioned signals in optical recordings of a rat heart. (A),(B) Still frames with color-coded pixels corresponding to the AP waveforms. (C),(E),(G) Signals obtained from iDS camera. (D),(F),(H) Signals obtained from the MiCAM camera.

In order to verify the accuracy of the conditioned signal waveform we have compared the mouse APD measured by the two cameras in control (n=6) and during administration of Ito blocker 4-aminopyridine (5.6mM, n=6). The comparison at 150 ms PCL is summarized in Fig 5. APD80 measurements by two cameras differed by 9 ± 9 ms in control and 4 ± 4 ms in 4-AP. The difference is partially due to the fact that recordings were not simultaneous and the field of view was slightly different. However, we found no statistically significant differences between APD measured by the cameras (paired t-test: $p = 0.101$ in control, $p = 0.058$ with 4AP; unpaired t-test: $p = 0.264$ in control, $p = 0.681$ with 4AP). It was possible to measure drug effect by the cheaper system: the iDS camera system registered 18 ± 3 ms action potential prolongation by 4-AP ($p = 0.0003$, paired t-test, Fig 5) which corresponds to low concentration 4-AP measurements in isolated cell experiments [17].

Fig 5. Comparison of APD measured by iDS and MiCAM. Comparison was made for a range of hearts (n=6) at PCL = 150ms in control and in presence of 5.6mM 4AP. Statistically significant differences are marked by an asterisk (paired t-test).

The APD restitution is depicted in Fig 6A**.** We did observe the reduction of APD with decreasing PCL with both cameras: over a change of PCL from 150 ms to 80 ms mean APD has decreased by 20 ms according to iDS and by 22 ms according to MiCAM, corresponding to relatively shallow slope of the restitution of the mouse heart [26,27].

Fig 6. APD and CV restitution curves. (A) APD80 restitution in control and in presence of 5.6 mM 4AP and (B) longitudinal/transversal CV restitution measured by iDS and MiCAM cameras.

Fig 7 and Fig 8 show comparisons of activation maps (A, C) and APD maps (B, D) measured in mouse and rat heart by iDS and MiCAM. Since the depolarization phase is less prone to noise, activation sequence and, consequently, CV could be determined more accurately than APD with the iDS camera. Root mean square deviation (RMSD) between measurements by two cameras was *4 cm/s* for longitudinal CV and 2 cm/s for transversal CV (Fig 6B). The CV restitution measurements with iDS camera were consistent with previous studies [28,29] with a slight reduction in CV when pacing frequency was increased (or PCL reduced). For example, at PCL=150 ms longitudinal CV was 51 ± 4 cm/s, transversal CV was

189 29 ± 3 cm/s; while at PCL=90 ms longitudinal CV was 47 ± 3 cm/s, transversal CV was 25 ±
190 3 cm/s, which is close to previously published measurements [28,29].

191 **Fig 7. Comparison of activation maps and APD maps recorded by iDS and**
192 **MiCAM.** (A) Mouse heart activation sequence measured by iDS camera. (B) Mouse heart
193 APD map measured by iDS camera. (C) Activation sequence measured by MiCAM camera.
194 (D) APD map measured by MiCAM camera. Pacing electrode location is marked by the
195 lightning symbol, black and orange arrows mark the directions for longitudinal and transversal
196 conduction velocities, correspondingly.

197 **Fig 8. Comparison of activation maps and APD maps captured by iDS and**
198 **MiCAM.** (A) Rat heart activation sequence measured by iDS camera. (B) Rat heart APD map
199 measured by iDS camera. (C) Activation sequence measured by MiCAM camera. (D) APD
200 map measured by MiCAM camera. Pacing electrode location is marked by the lightning
201 symbol.

202 It should also be noted that the rat heart (Fig 8) was paced from the atrioventricular
203 groove. We can see independent AP propagation in the atria and ventricles from the pacing
204 electrode, which demonstrates that both atrial and ventricular activation sequence can be
205 accurately recorded with a cheaper optical mapping system.

206 # Discussion

207 We have implemented a low-cost open-source optical mapping system, capable of 977
208 FPS 200x200 pixel imaging. The total system price, as shown in S1 Table, is below US$5,000
209 including the light source, at the time of publication, while the gold standard Micam Ultima-L
210 system used in this study for comparison is priced at or above US$100,000. It should be noted
211 that the main goal of the study was to test the iDS camera capabilities and limitations. Therefore,
212 we kept all components apart from camera and optics equal in both optical mapping system
213 setups. As a consequence, the LED we used for die excitation was the most expensive part of
214 the optical mapping system, while the camera and lens themselves were priced below
215 US$1,000.

In our study we have shown that iDS system recordings are of sufficient quality for AP waveform (Figs 3,4), activation sequence (Figs 7A, 8A) and CV (Fig 6B) measurements, at 1/100 price. Low signal amplitude resulted in SNR of raw recordings of 0.5±0.4 for the mouse heart and 2.0 ± 0.7 for the rat heart. After signal conditioning, including binning and ensemble averaging, SNR significantly improved to 16±10 for mouse heart and 10±3 for a rat heart making it close to MiCAM recordings (Fig 2). As noted above, depolarization phase recording is less prone to noise then relatively slow repolarization. Consequently, activation sequence and CV measurements by iDS system were robust: RMSD between corresponding recordings by two cameras was equal to 4 cm/s. On the other hand the difference between APD measurements was more pronounced. For example, iDS measurements at 150 ms PCL w/o drug were on average 9 ms longer than MiCAM measurements (Fig 6A). This difference is, in part, due to the distortion of the depolarisation phase and resting potential level by noise. The latter affects the 80% repolarization level hampering the comparison between cameras with different SNR. However, in the worst-case scenario, the difference between APD measurements was 22 ms despite the fact that SNR was high in the iDS recording (SNR equals 25 for this heart, while the average SNR was 16, representative SNR maps for all recordings can be found in S2 Fig). We conclude that largest deviations between the recordings are actually caused by the fact that recordings were not simultaneous, and the field of view was different for the two cameras. Despite this difference between the recordings, we have demonstrated that the iDS system is feasible for drug effect measurements. In particular, we have shown significant prolongation of APD by the transient outward current blocker 4-AP (Fig. 5, 18±3 ms, n=5, p=0.0003, paired t-test). Similar APD prolongation at low drug concentrations was reported previously in isolated mouse ventricular cells[17] and small tissue atrial preparations[30].

Previously Lee et al. had already demonstrated iDS low-cost cameras for panoramic optical mapping [14], using UI-3360CP camera at 1,000 FPS, 160x220 pixels, yielding SNR of about 35 for pig hearts and SNR of about 10 for rabbit hearts at 400 FPS, but the software used in the study was not openly available and the method was not widely disseminated in cardiovascular research community. During the preparation of this publication, Lee et al. published a report of a complete and low-cost optical mapping system, which includes a Langendorff perfusion system complete with pumps and a thermostat with custom controllers,

as well as an LED system and an open-source code for low-cost iDS camera [31]. However, this competing software is not readily compatible with currently available GUI-based signal conditioning and analysis software [9,32–34] and it lacks a graphical user interface suggesting the use of separate *uEye cockpit* application to refocus the camera, adjust the LED intensity and camera gain. The authors presented recordings at 500 FPS, which is often not enough for rodent hearts, in which the entire heart activation takes about 10 ms (Figs 7, 8). The validation of the system in the study was conducted on large mammals, pig and rabbit hearts, while lacking direct comparison to established optical mapping systems. It remains to be shown that their method is applicable to popular rodent heart models.

In our work, we focused on the development of optical mapping solution that can be used by biomedical researchers and educators lacking programming or electrical engineering skills. We present a custom open-source software that provides a graphical user interface, convenient interactive camera settings and a real-time viewfinder feed (S1 Fig) and is compatible with established open source Rhythm analysis software that was used through the past decade by many research laboratories [9,32]. The solution including camera and custom open-source software was proven to produce accurate recordings by direct comparison to a specialized optical mapping system. Moreover, our study demonstrates that AP measurements on mouse and rat ventricles (thickness 1.5 and 1.9 mm) and atria are possible, while the previous studies focused on much larger mammals: pig (thickness 20 mm) and rabbit ventricles (thickness 5 mm) [35-38]. While larger hearts yield higher signal intensity, we have demonstrated that at 977 FPS, 200x200 pixels the iDS solution is sufficient not only for AP waveform recordings in small rodent hearts, but also for accurate measurements of both longitudinal and transversal CV in the mouse heart. The high flexibility of software also allows for long recordings. We have tested up to five minutes recordings. It may prove to be essential for the measurement of slower NADH changes during ischemia/reperfusion studies[7,39]. Signal acquisition and processing software used in this study are open-source and distributed under MIT license (the links are provided in the Appendix).

One of the limitations of the presented solution is a requirement of a wide-angle lens. UI-3130CP has a 1/3.6” sensor, while the effective size was reduced to 1x1mm in order to increase the camera frame rate. Therefore, the lens used in the study (Pentax 6mm TV lens)

277 provided only a 9.2 degrees field of view, which is optimal for the hearts of small rodents such
278 as rats and mice, but a different lens or a tandem optical system should be designed for larger
279 mammals.

280 References

281 1. Boukens BJ, Efimov IR. A century of optocardiography. IEEE Rev Biomed Eng.
282 2014;7: 115–125.

283 2. Cohen LB, Salzberg BM. Optical measurement of membrane potential. Reviews of
284 Physiology, Biochemistry and Pharmacology. 1978. pp. 35–88. doi:10.1007/3-540-
285 08907-1_2

286 3. Salzberg BM, Davila HV, Cohen LB. Optical recording of impulses in individual
287 neurones of an invertebrate central nervous system. Nature. 1973;246: 508–509.

288 4. Salama G, Morad M. Merocyanine 540 as an optical probe of transmembrane electrical
289 activity in the heart. Science. 1976;191: 485–487.

290 5. Loew LM. Design and characterization of electrochromic membrane probes. J Biochem
291 Biophys Methods. 1982;6: 243–260.

292 6. Takahashi A, Camacho P, Lechleiter JD, Herman B. Measurement of intracellular
293 calcium. Physiol Rev. 1999;79: 1089–1125.

294 7. Salama G, Lombardi R, Elson J. Maps of optical action potentials and NADH
295 fluorescence in intact working hearts. Am J Physiol. 1987;252: H384–94.

296 8. Efimov IR, Huang DT, Rendt JM, Salama G. Optical mapping of repolarization and
297 refractoriness from intact hearts. Circulation. 1994. pp. 1469–1480.
298 doi:10.1161/01.cir.90.3.1469

299 9. Cathey B, Obaid S, Zolotarev AM, Pryamonosov RA, Syunyaev RA, George SA, et al.
300 Open-Source Multiparametric Optocardiography. Sci Rep. 2019;9: 721.

301 10. Lin SF, Wikswo JP. Panoramic optical imaging of electrical propagation in isolated
302 heart. J Biomed Opt. 1999;4: 200–207.

303 11. Gloschat C, Aras K, Gupta S, Faye NR, Zhang H, Syunyaev RA, et al. RHYTHM: An
304 Open Source Imaging Toolkit for Cardiac Panoramic Optical Mapping. Sci Rep. 2018;8:
305 2921.

306 12. Bernus O, Mukund KS, Pertsov AM. Detection of intramyocardial scroll waves using
307 absorptive transillumination imaging. J Biomed Opt. 2007;12: 014035.

13. Ripplinger CM. Panoramic Optical Imaging of Cardiac Arrhythmias. Cardiac Mapping. 2012. pp. 90–97. doi:10.1002/9781118481585.ch10

14. Lee P, Calvo CJ, Alfonso-Almazán JM, Quintanilla JG, Chorro FJ, Yan P, et al. Low-Cost Optical Mapping Systems for Panoramic Imaging of Complex Arrhythmias and Drug-Action in Translational Heart Models. Sci Rep. 2017;7: 43217.

15. Witkowski FX, Leon LJ, Penkoske PA, Giles WR, Spano ML, Ditto WL, et al. Spatiotemporal evolution of ventricular fibrillation. Nature. 1998;392: 78–82.

16. Lang D, Sulkin M, Lou Q, Efimov IR. Optical mapping of action potentials and calcium transients in the mouse heart. J Vis Exp. 2011. doi:10.3791/3275

17. Fiset C, Clark RB, Larsen TS, Giles WR. A rapidly activating sustained K+ current modulates repolarization and excitation-contraction coupling in adult mouse ventricle. J Physiol. 1997;504 (Pt 3): 557–563.

18. Li GR, Feng J, Wang Z, Fermini B, Nattel S. Comparative mechanisms of 4-aminopyridine-resistant Ito in human and rabbit atrial myocytes. Am J Physiol. 1995;269: H463–72.

19. Näbauer M, Beuckelmann DJ, Erdmann E. Characteristics of transient outward current in human ventricular myocytes from patients with terminal heart failure. Circ Res. 1993;73: 386–394.

20. Wegener JW, Peiter A, Sampson SR, Nawrath H. Mechanism of block by 4-aminopyridine of the transient outward current in rat ventricular cardiomyocytes. J Cardiovasc Pharmacol. 1998;32: 134–138.

21. Castle NA, Slawsky MT. Characterization of 4-aminopyridine block of the transient outward K+ current in adult rat ventricular myocytes. J Pharmacol Exp Ther. 1993;265: 1450–1459.

22. Simurda J, Simurdová M, Christé G. Use-dependent effects of 4-aminopyridine on transient outward current in dog ventricular muscle. Pflugers Arch. 1989;415: 244–246.

23. Kostadinova I, Danchev N. 4-aminopyridine – the new old drug for the treatment of neurodegenerative diseases. Pharmacia. 2019. pp. 67–74. doi:10.3897/pharmacia.66.e35976

24. Huang CL-H. Murine Electrophysiological Models of Cardiac Arrhythmogenesis. Physiol Rev. 2017;97: 283–409.

25. Bayly PV, KenKnight BH, Rogers JM, Hillsley RE, Ideker RE, Smith WM. Estimation of conduction velocity vector fields from epicardial mapping data. IEEE Trans Biomed Eng. 1998;45: 563–571.

26. Knollmann BC, Schober T, Petersen AO, Sirenko SG, Franz MR. Action potential

characterization in intact mouse heart: steady-state cycle length dependence and electrical restitution. Am J Physiol Heart Circ Physiol. 2007;292: H614–21.

27. Knollmann BC, Katchman AN, Franz MR. Monophasic action potential recordings from intact mouse heart: validation, regional heterogeneity, and relation to refractoriness. J Cardiovasc Electrophysiol. 2001;12: 1286–1294.

28. Stein M, van Veen TAB, Hauer RNW, de Bakker JMT, van Rijen HVM. A 50% Reduction of Excitability but Not of Intercellular Coupling Affects Conduction Velocity Restitution and Activation Delay in the Mouse Heart. PLoS ONE. 2011. p. e20310. doi:10.1371/journal.pone.0020310

29. Eloff BC, Lerner DL, Yamada KA, Schuessler RB, Saffitz JE, Rosenbaum DS. High resolution optical mapping reveals conduction slowing in connexin43 deficient mice. Cardiovasc Res. 2001;51: 681–690.

30. Golovko V, Gonotkov M, Lebedeva E. Effects of 4-aminopyridine on action potentials generation in mouse sinoauricular node strips. Physiological Reports. 2015. p. e12447. doi:10.14814/phy2.12447

31. Marina-Breysse M, García-Escolano A, Vila-García J, Reale-Nosei G, Alfonso-Almazán JM, Yan P, et al. A Complete and Low-Cost Cardiac Optical Mapping System in Translational Animal Models. Front Physiol. 2021;12: 696270.

32. Laughner JI, Ng FS, Sulkin MS, Arthur RM, Efimov IR. Processing and analysis of cardiac optical mapping data obtained with potentiometric dyes. Am J Physiol Heart Circ Physiol. 2012;303: H753–65.

33. O'Shea C, Holmes AP, Yu TY, Winter J, Wells SP, Correia J, et al. ElectroMap: High-throughput open-source software for analysis and mapping of cardiac electrophysiology. Sci Rep. 2019;9: 1389.

34. Li X, Roney CH, Handa BS, Chowdhury RA, Niederer SA, Peters NS, et al. Standardised Framework for Quantitative Analysis of Fibrillation Dynamics. Sci Rep. 2019;9: 16671.

35. Forman DE, Cittadini A, Azhar G, Douglas PS, Wei JY. Cardiac morphology and function in senescent rats: gender-related differences. J Am Coll Cardiol. 1997;30: 1872–1877.

36. Vetter FJ, McCulloch AD. Three-dimensional analysis of regional cardiac function: a model of rabbit ventricular anatomy. Progress in Biophysics and Molecular Biology. 1998. pp. 157–183. doi:10.1016/s0079-6107(98)00006-6

37. Huang SY, Tsou HL, Chiu YT, Wu JJ, Lin JH, Yang PC, et al. Statistical method for characterization of hypertrophic cardiomyopathy by use of morphologic and pathologic measurements in pigs (Sus scrofa domestica). Lab Anim Sci. 1999;49: 276–282.

379 38. Doevendans P. Cardiovascular phenotyping in mice. Cardiovascular Research. 1998. pp.
380 34–49. doi:10.1016/s0008-6363(98)00073-x

381 39. Mercader M, Swift L, Sood S, Asfour H, Kay M, Sarvazyan N. Use of endogenous
382 NADH fluorescence for real-time in situ visualization of epicardial radiofrequency
383 ablation lesions and gaps. Am J Physiol Heart Circ Physiol. 2012;302: H2131–8.

384

385 Supporting information

386 **S1 Fig. Interactive image acquisition software.** Screenshots of image acquisition
387 software. Real-time viewfinder feed allows the user to adjust settings when signal amplitude
388 is too low (B,C) or oversaturating (D).

389 **S2 Fig**. **SNR maps.** SNR maps for conditioned recordings of 6 mouse hearts recorded
390 with iDS camera at PCL = 150 ms.

391 **S1 Table. Component prices in the MiCAM Ultimate-L system and the system**
392 **presented in this study.**

393 **S1 Text. Software links and supporting figures.**

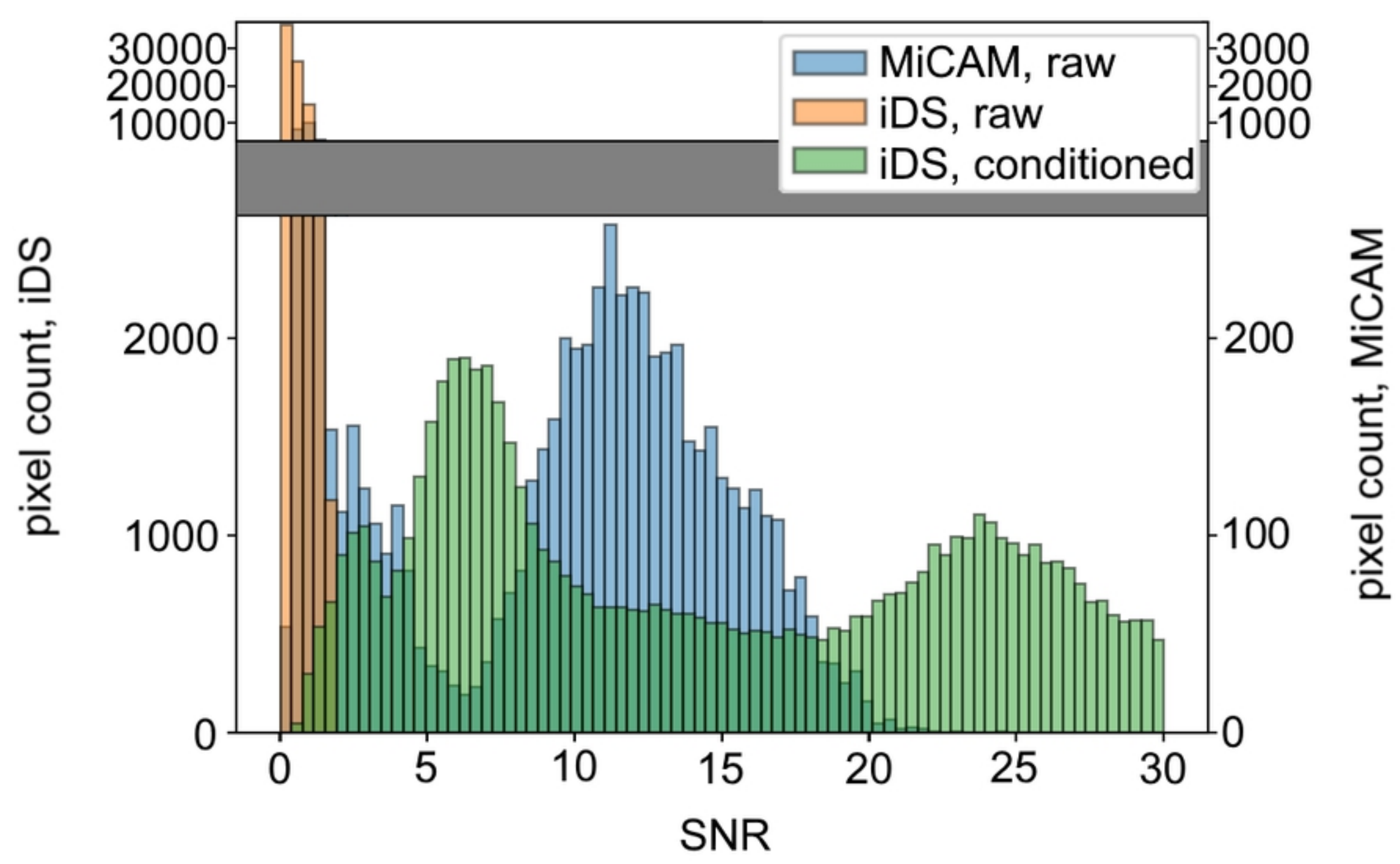
MiCAM, raw
iDS, raw
iDS, conditioned
pixel count, iDS
pixel count, MiCAM
SNR
30000
20000
10000
2000
1000
0
3000
2000
1000
200
100
0
0
5
10
15
20
25
30

Figure 2

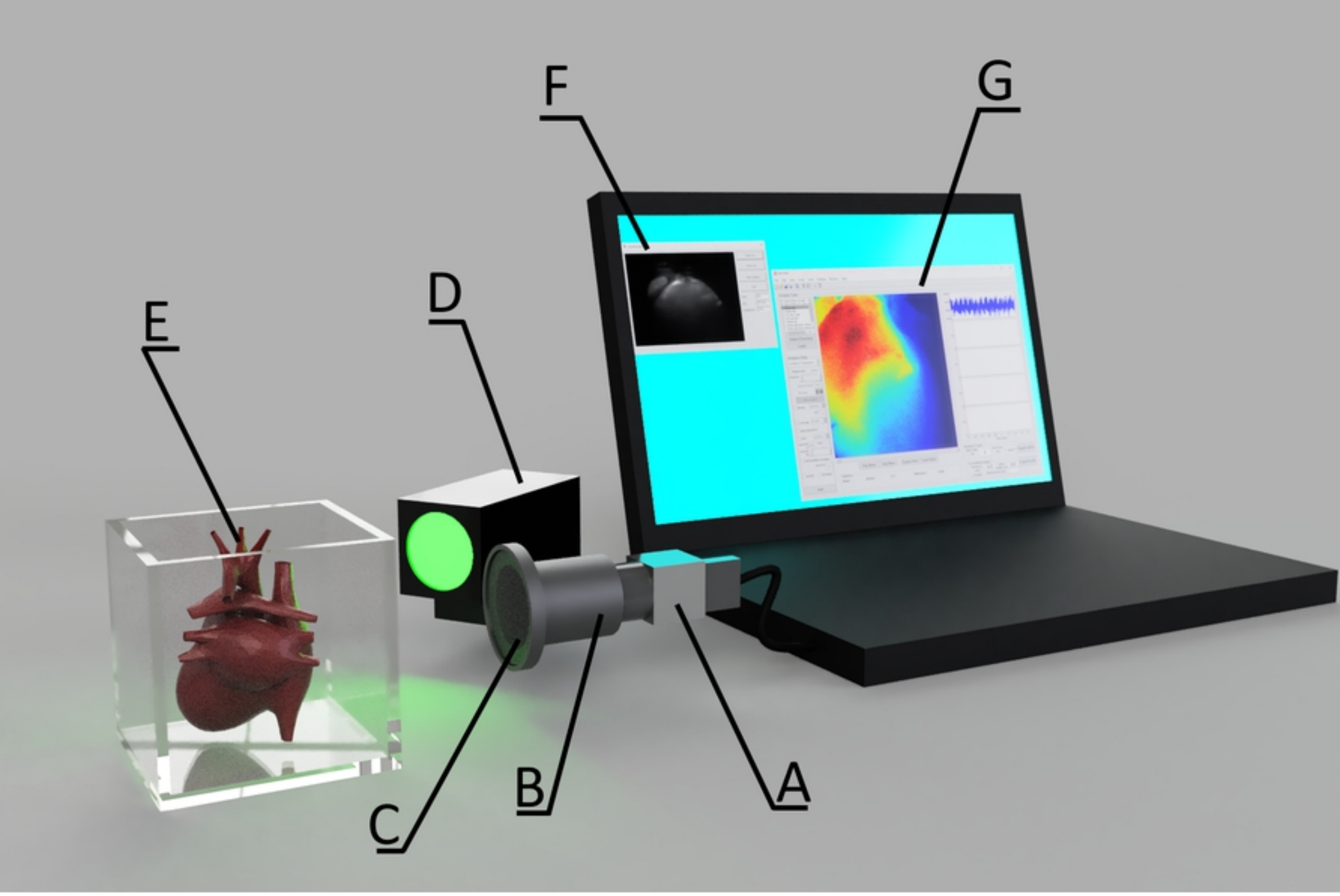

Figure 1

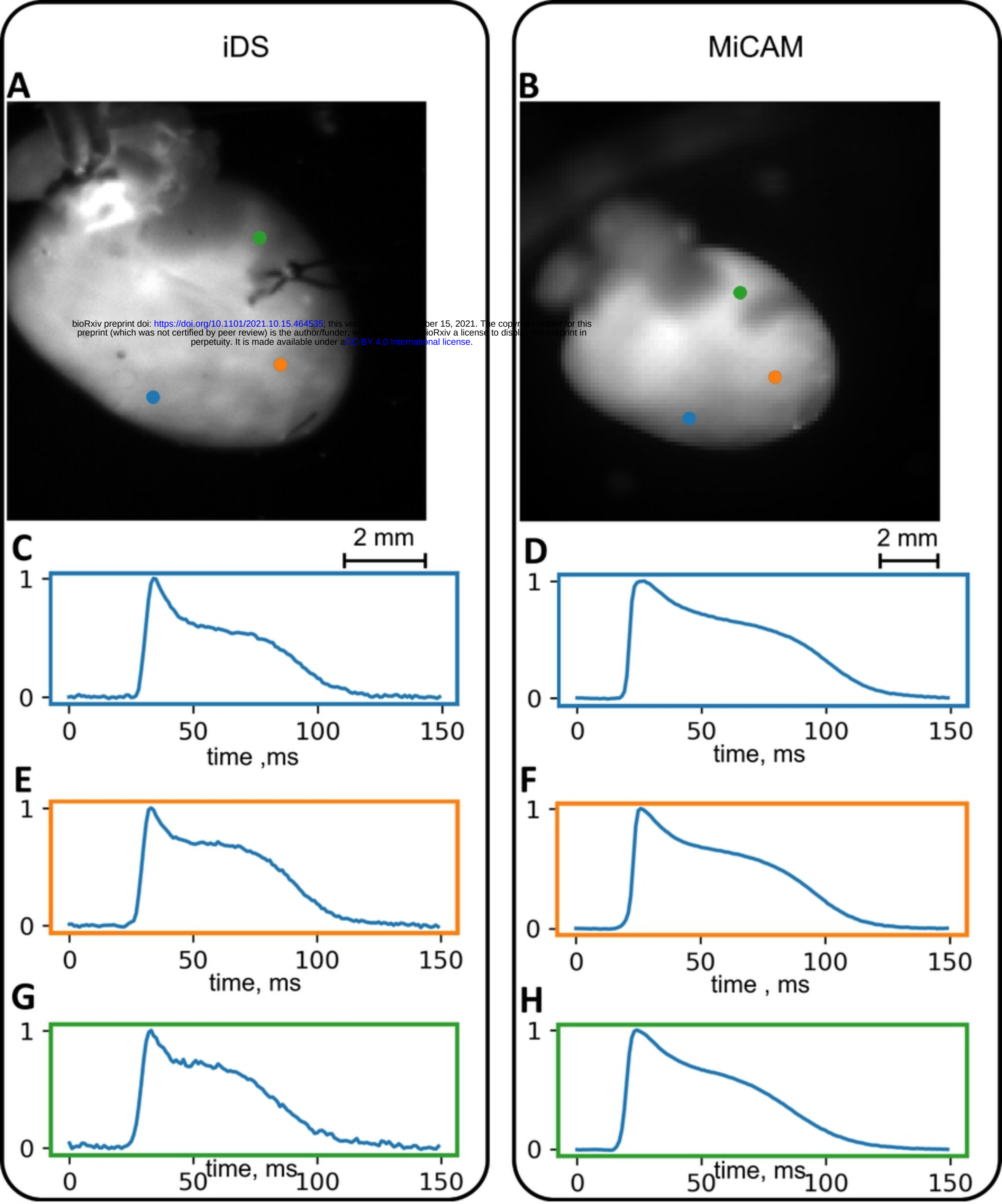

Figure 3

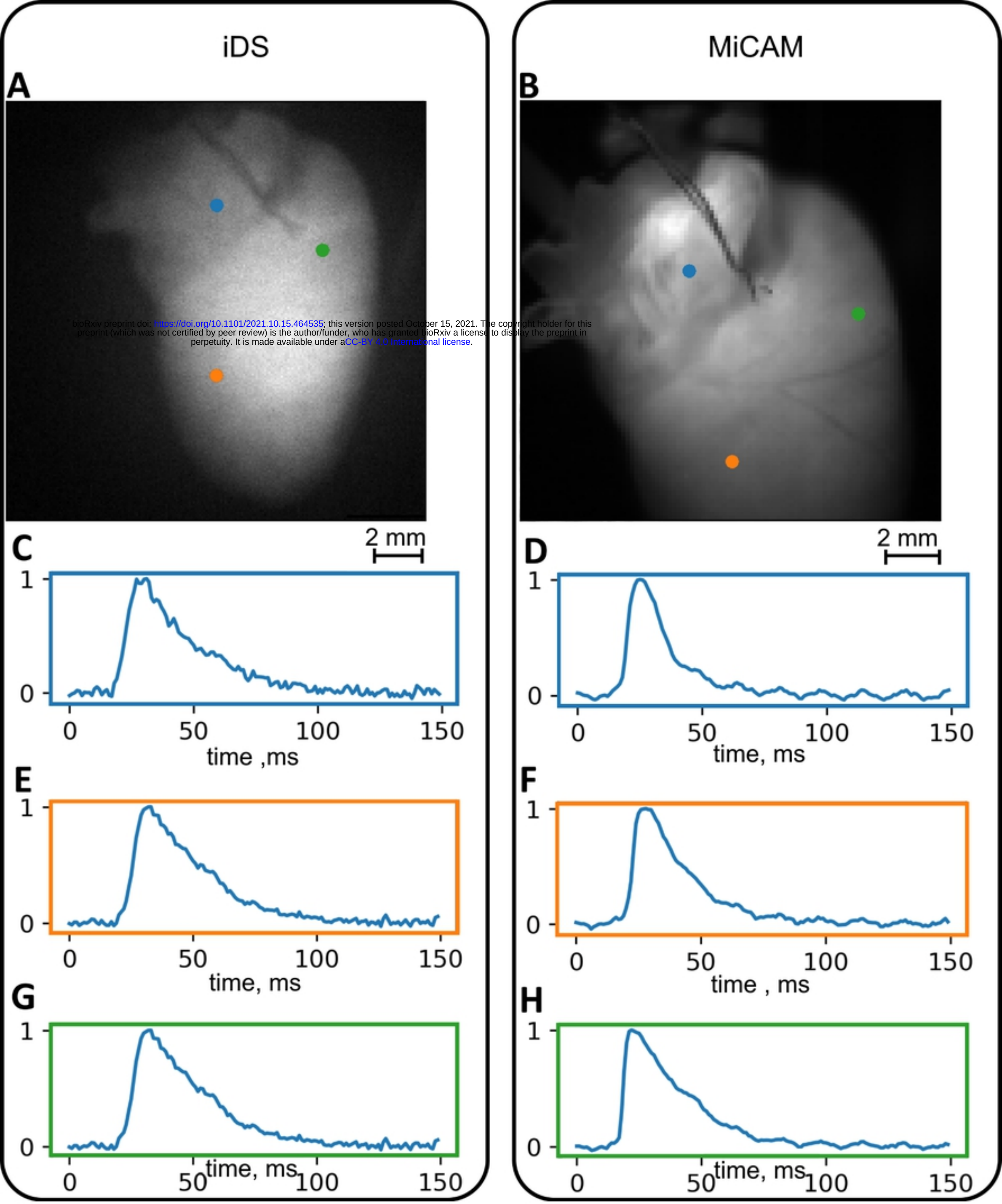

Figure 4

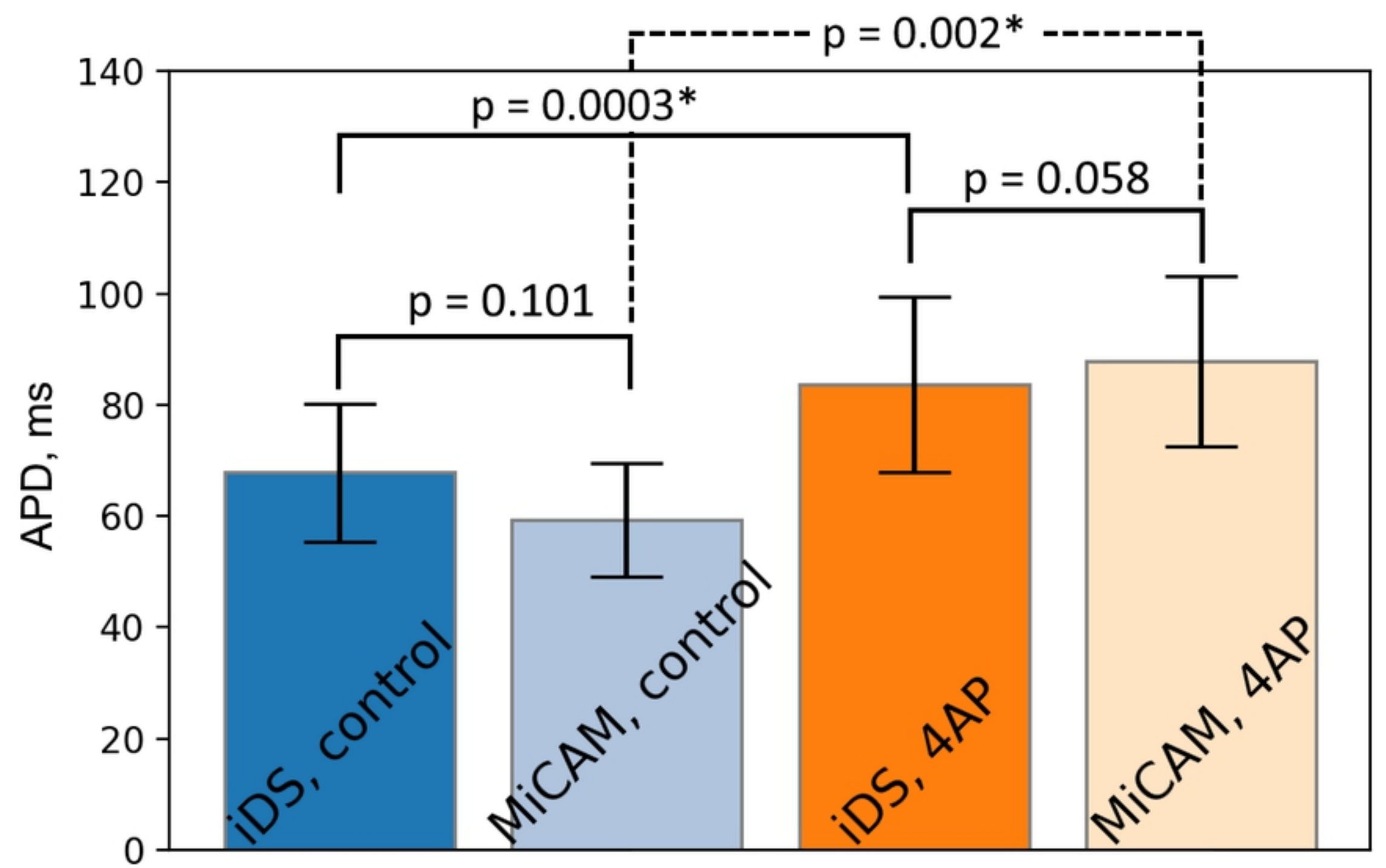
p = 0.002*
p = 0.0003*
p = 0.058
p = 0.101
140
120
100
80
60
40
20
0
APD, ms
iDS, control
MiCAM, control
iDS, 4AP
MiCAM, 4AP

Figure 5

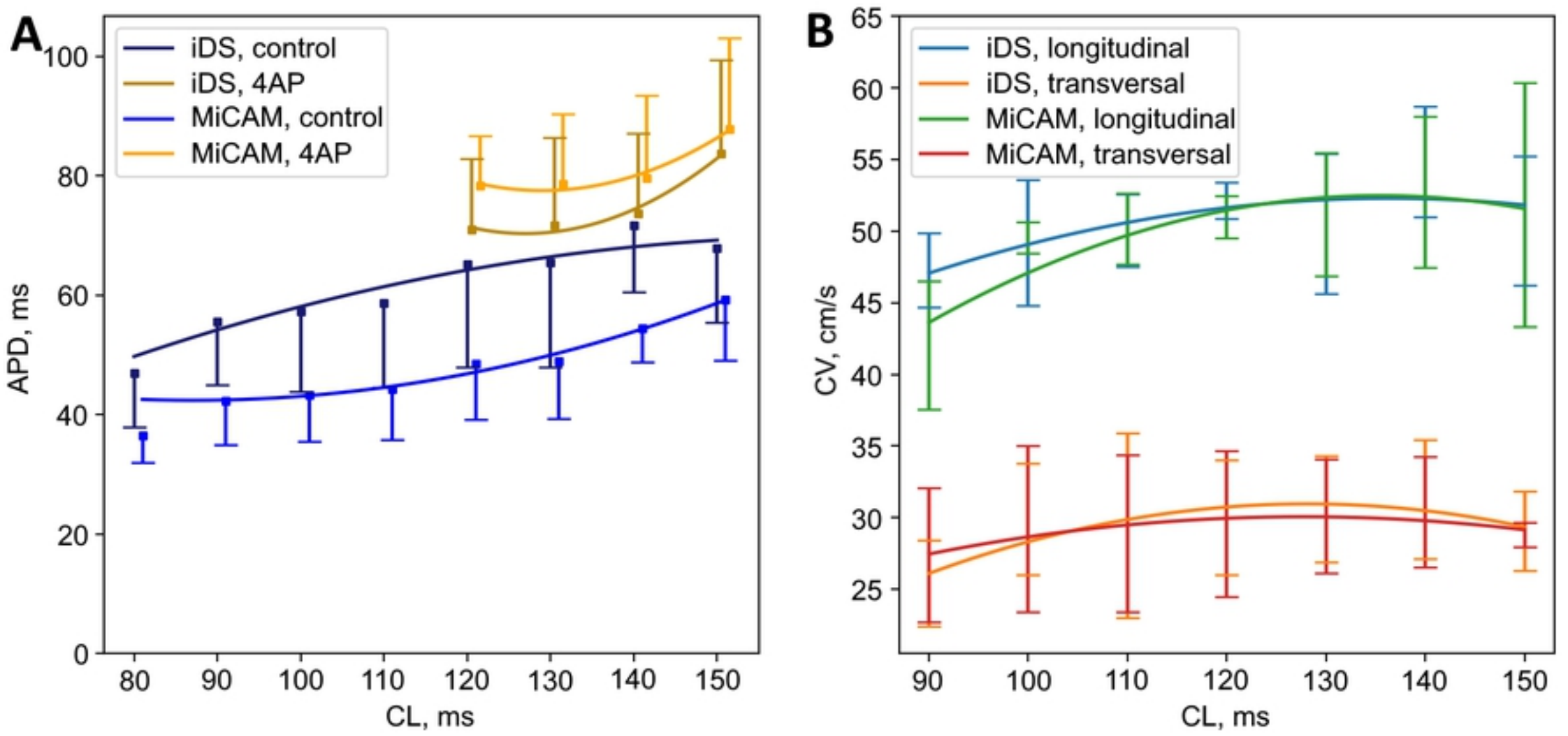
A
iDS, control
iDS, 4AP
MiCAM, control
MiCAM, 4AP
APD, ms
CL, ms
B
iDS, longitudinal
iDS, transversal
MiCAM, longitudinal
MiCAM, transversal
CV, cm/s
CL, ms

Figure 6

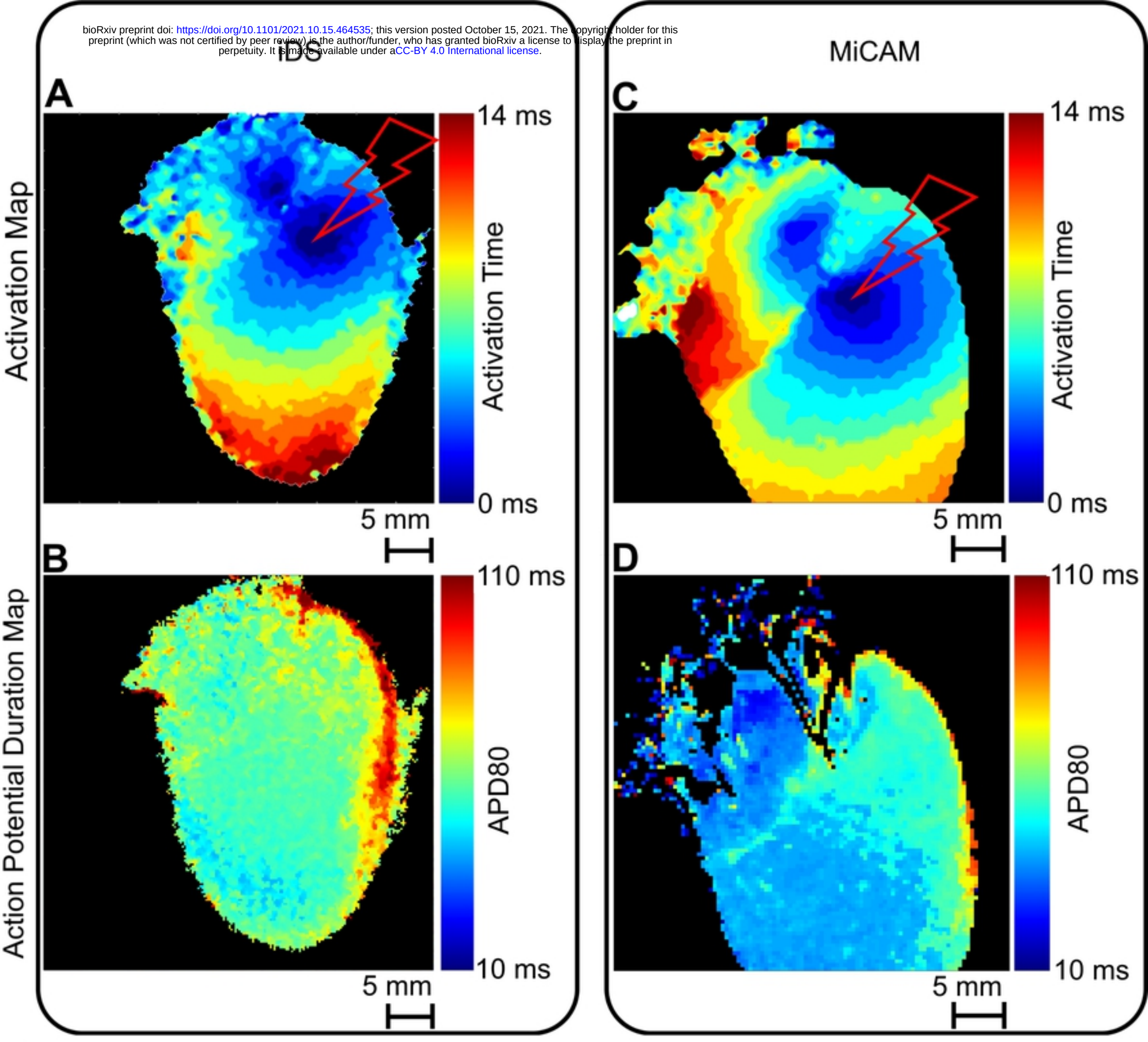

Figure 8

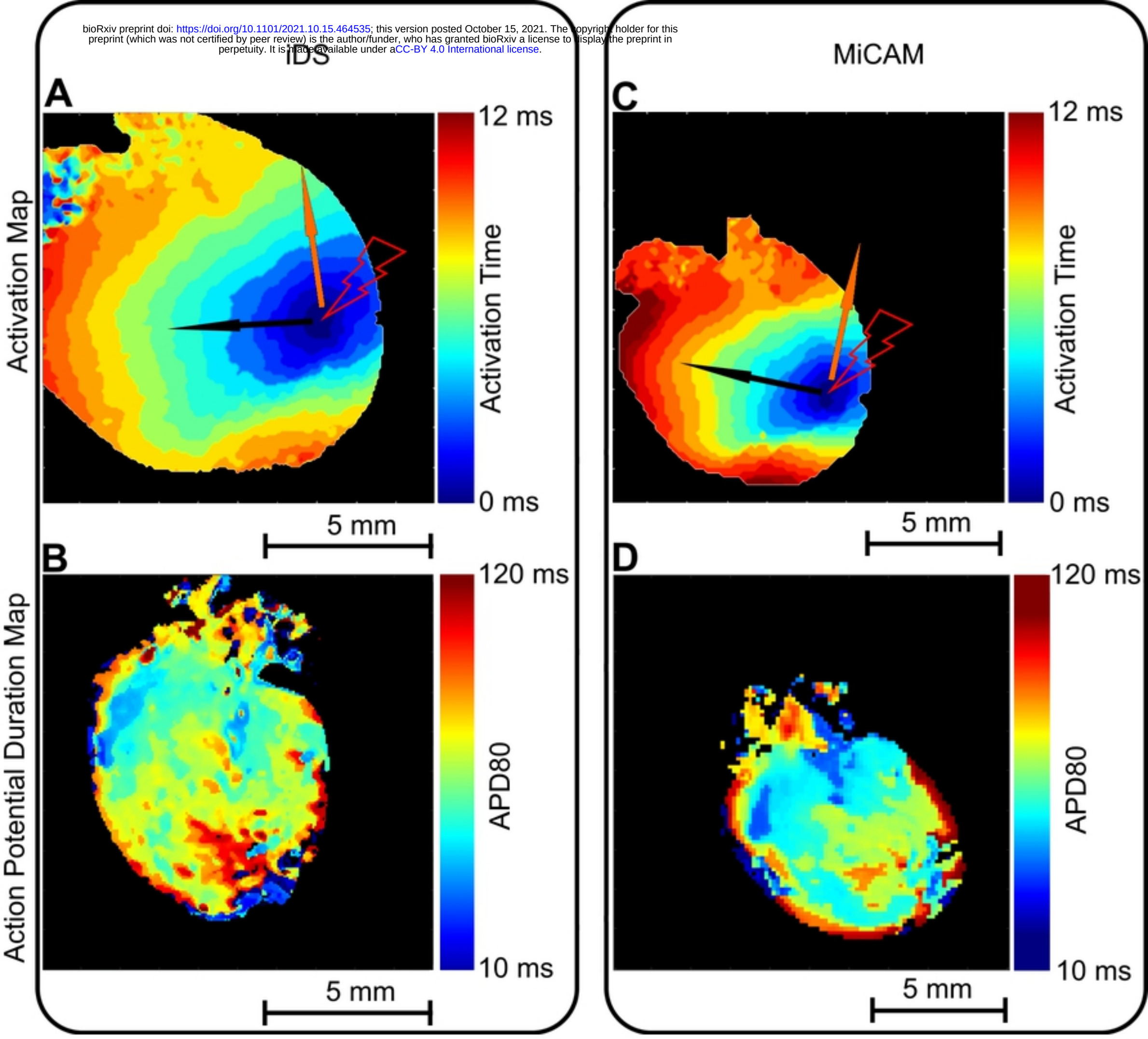

Figure 7